Astronomy & Astrophysics manuscript no. aa11176
February 9, 2009

Detection of X-rays from the jet-driving Symbiotic Star MWC 560

Matthias Stute[1] and Raghvendra Sahai[2]

[1] IASA and Section of Astrophysics, Astronomy and Mechanics, Department of Physics, University of Athens, Panepistimiopolis, 15784 Zografos, Athens, Greece
[2] Jet Propulsion Laboratory, California Institute of Technology, 4800 Oak Grove Drive, Pasadena, CA 91109, USA

Received 17 October 2008; accepted 01 February 2009

ABSTRACT

Aims. We report the detection of X-ray emission from the jet-driving symbiotic star MWC 560.
Methods. We observed MWC 560 with XMM-Newton for 36 ks. We fitted the spectra from the EPIC pn, MOS1 and MOS2 instruments with XSPEC and examined the light curves with the package XRONOS.
Results. The spectrum can be fitted with a highly absorbed hard X-ray component from an optically-thin hot plasma, a Gaussian emission line with an energy of 6.1 keV and a less absorbed soft thermal component. The best fit is obtained with a model in which the hot component is produced by optically thin thermal emission from an isobaric cooling flow with a maximum temperature of 61 keV, which might be created inside an optically-thin boundary layer on the surface of the accreting with dwarf. The derived parameters of the hard component detected in MWC 560 are in good agreement with similar objects as CH Cyg, SS7317, RT Cru and T CrB, which all form a new sub-class of symbiotic stars emitting hard X-rays. Our previous numerical simulations of the jet in MWC 560 showed that it should produce detectable soft X-ray emission. We infer a temperature of 0.17 keV for the observed soft component, i.e. less than expected from our models. The total soft X-ray flux (i.e. at < 3 keV) is more than a factor 100 less than predicted for the propagating jet soon after its birth (< 0.3 yr), but consistent with the value expected due its decrease with age. The ROSAT upper limit is also consistent with such a decrease. We find aperiodic or quasi-periodic variability on timescales of minutes and hours, but no periodic rapid variability.
Conclusions. All results are consistent with an accreting white dwarf powering the X-ray emission and the existence of an optically-thin boundary layer around it.

Key words. accretion, accretion disk – binaries: symbiotic – stars: individual (MWC 560=V694 Mon) – stars: white dwarfs – X-rays: stars

1. Introduction

Highly collimated fast outflows or jets are common in many astrophysical objects of different sizes and masses: active galactic nuclei (AGN), X-ray binaries (XRBs), young stellar objects (YSO), pre-planetary nebulae (PPN), supersoft X-ray sources and symbiotic stars. However, there are still open questions concerning the formation of jets.

In current jet formation models, accretion disks and magnetic fields play a key role. In their analytical model, Blandford & Payne (1982) invoked magneto-centrifugal acceleration along magnetic field lines threading an accretion disk – the poloidal magnetic field component brakes the disk matter and accelerates it into the jet and the toroidal component collimates the flow.

Symbiotic stars are ideal test beds for studying the formation and propagation of jets in binary systems where an accretion disk is believed to exist around a white dwarf (WD). Symbiotic stars are interacting binaries with orbital periods in the range of years; the cool component is a red giant (RG), the hot component a WD (with Teff ∼ 50000 – 200000 K). Both stars show mass loss through supersonic winds. Wind material from the RG is captured by the WD to form an accretion disk. Prominent jets have been observed in symbiotic stars, in stark contrast to other binary systems with WD companions, like cataclysmic variables which also harbor accretion disks, yet show no jets.

About 200 symbiotic stars are known (e.g. Belczynski et al. 2000), but jets have been detected at different wavelengths only in 10 out of them (Brocksopp et al. 2004). The most famous systems are R Aquarii, CH Cygni and MWC 560. X-ray observations provide a direct probe of the two most important components of jet-driving systems: the bow and internal shocks of the jet and the central parts of the jet engine, where gas is being accreted for powering the jet. Up to now, R Aqr and CH Cyg are the only two jets of symbiotic stars which are detected in X-rays.

R Aquarii, with a distance of about 200 pc, is one of the nearest symbiotic stars and a well known jet source. The jet has been extensively observed in the optical and at radio wavelengths (e.g. Solf & Ulrich 1985; Paresce & Hack 1994; Hollis et al. 1985a,b). It shows a rich morphology with hints of pulsed ejection. Furthermore, R Aqr is the first jet in a symbiotic system, which was detected in X-rays (Viotti et al. 1987; Hünsch et al. 1998; Kellogg et al. 2001). The spectra of the jets are consistent with a soft component with $kT \sim 0.25$ keV. The central source shows a supersoft blackbody emission with $kT \sim 0.18$ keV and a Fe Kα line at 6.4 keV which suggests the presence of a hard source near the hot star. Recently, Kellogg et al. (2007) reported on five years of observations with Chandra and were able to measure the proper motion of knots in the NE jet of about 600 km s^{-1}. Nichols et al. (2007) investigated the X-ray emission from the inner 500 AU of this system and were able to observe a hard thermal component with a temperature of 6.8 keV.

Send offprint requests to: Matthias Stute,
e-mail: mstute@phys.uoa.gr

In 1984/85, CH Cygni showed a strong radio outburst, during which a double-sided jet with multiple components was ejected (Taylor et al. 1986). This event allowed an accurate measurement of the jet velocity near 1500 km s^{-1}. In HST observations (Eyres et al. 2002), arcs can be detected that also could be produced by episodic ejection events. X-ray emission was first detected by EXOSAT (Leahy & Taylor 1987), and subsequent ASCA observations revealed a complex X-ray spectrum with two soft components (kT = 0.2 and 0.7 keV) associated with the jet, an absorbed hard component (7.3 keV) and a Fe Kα line (Ezuka et al. 1998). Analysis of archival Chandra ACIS data by Galloway & Sokoloski (2004) revealed faint extended emission to the south, aligned with the optical and radio jets seen in HST and VLA observations. An apparent decline of the hard X-ray component has been observed with the US-Japanese X-ray satellite Suzaku by Mukai et al. (2007). Recently, Karovska et al. (2007) reported the detection of multiple spatial components, including an arc, in the archival Chandra images.

In both objects, hints of variability of the hard X-ray component were found with periods of 1734s in R Aqr (Nichols et al. 2007) and 130s in CH Cyg (Ezuka et al. 1998), however, not with high confidence levels. If present, these variabilities can be interpreted as the Keplerian period at the magnetospheric radius, where the accretion disk is truncated by a strong magnetic field of the WD.

While these two objects are seen at high inclinations, in MWC 560 (or V694 Mon) the jet axis is practically parallel to the line of sight (Tomov et al. 1990; Schmid et al. 2001). This special orientation allows one to observe the outflowing gas as line absorption in the source spectrum. With such observations the radial velocity and the column density of the outflowing jet gas close to the source has been investigated in great detail. In particular the acceleration and evolution of individual outflow components and jet pulses has been probed with spectroscopic monitoring programs, as described in Schmid et al. (2001). Using this optical data, sophisticated numerical models of this pulsed propagating jet have been developed (Stute, Camenzind & Schmid 2005; Stute 2006). A number of hydrodynamical simulations (with and without cooling) were made in which the jet density and velocity during the pulses were varied. The basic model absorption line profiles in MWC 560 as well as the mean velocity and velocity-width are in good agreement with the observations. The evolution of the time-varying high velocity absorption line-components is also well modeled. These models not only fit the MWC 560 data, but are also able to explain properties of jets in other symbiotic systems such as the observed velocity and temperature of the CH Cyg jet. Until recently, no hydrodynamical models existed for explaining the X-ray emission from symbiotic stars, thus as a first step we have therefore used our existing simulations, which fit MWC 560, for understanding the observed X-ray emission properties of CH Cyg and R Aqr and the expected properties of MWC 560 (Stute & Sahai 2007). In our models, the jet emits two soft one-temperature components, similar to those seen in CH Cyg.

MWC 560 has not been detected in X-rays so far – only ROSAT observations have been available, with an upper limit of 7×10^{-4} counts s^{-1} (Mürset et al. 1997) corresponding to 8×10^{-15} ergs cm^{-2} s^{-1} (PIMMS). Here, finally, we report on the analysis of our recent *XMM-Newton* observations of MWC 560 and on the detection of X-ray emission from this object.

The remainder is organized as follows: in §2, we show details of the observations and the analysis of the data. After that we describe the results in §3. We end with a discussion and conclusions.

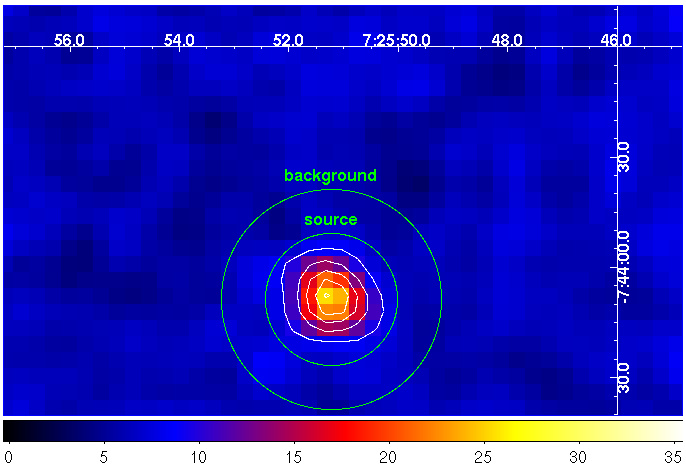

Fig. 1. *XMM-Newton* EPIC pn image (detail) of the field of MWC 560 in the 0.2–15 keV range. Also shown are the extraction regions for the source and the background events. Contour levels are 9, 12.6, 16.3 and 20 counts.

2. Observation and Analysis

The *XMM-Newton* X-ray observatory observed the field of MWC 560 for 33 ks in 2007 on September 27, from 02:17 UT to 12:22 UT (observation ID: 0501350101). The data were collected with the EPIC instrument, which consists of two MOS (Turner et al. 2001) and one pn (Strüder et al. 2001) cameras sensitive to photons with energies between 0.15 and 15 keV. The EPIC pn as well as EPIC MOS were operated in Full Window mode, i.e. with a field of view of 30'. Both the pn and MOS mounted the medium thickness filter. Simultaneously, the observations provided optical imaging from the Optical Monitor (OM; Mason et al. 2001). Because of a low count rate, the Reflection Grating Spectrograph data were not useful. Further details are given in Table 1.

All the data reduction was performed using the Science Analysis Software (SAS) software package[1] version 7.1. The raw observation data files were processed using standard pipeline tasks (epproc for pn, emproc for MOS data). We selected events with pattern 0–4 (only single and double events) for the pn and pattern 0–12 for the MOS, respectively, and applied the filter FLAG=0.

2.1. Spectral analysis

The source spectra were accumulated from a circular region (360 pixels radius, 18") centered on MWC 560, using the pn and also the MOS1 and MOS2 detectors. The background spectra were extracted from a source-free region of the same chip taken with an annulus centered on the source around the former region with an outer radius of 600 pixels (30", Fig. 1).

Spectral redistribution matrices and ancillary response files were generated using the SAS scripts rmfgen and arfgen, and spectra grouped with a minimum of 25 counts per energy bin were fed into the spectral fitting package XSPEC[2] version 12.4.0. Spectral channels having energies below 0.1 keV and bad channels were ignored.

[1] See http://xmm.vilspa.esa.es/.
[2] See http://heasarc.gsfc.nasa.gov/docs/xanadu/xspec/.

Table 1. Observations on September 27, 2007

Instrument	Filter	Duration (s)	UT Start Time	UT Stop Time
PN	Medium	34457	02:40:19	12:14:36
MOS1	Medium	36019	02:18:22	12:18:41
MOS2	Medium	36026	02:18:21	12:18:47

2.2. Timing analysis

We searched for variabilities in the X-ray emission from MWC 560 using the pn detector. Source photons were again selected from a circular region centered on MWC 560 with a radius of 360 pixels (18") and background photons from an annulus around the former region with an outer radius of 600 pixels (30", Fig. 1). Photon arrival times were converted to the solar system barycentre using the SAS task barycen.

We searched the data for pulsations over a wide period range using efsearch and powspec within the package XRONOS[3] version 5.21.

3. Results

3.1. Spectra

We find 624 counts in our source annuli in the EPIC pn detector, 150 counts in MOS1 and 137 counts in MOS2, respectively, all in the range of 0.2 – 15 keV. In the soft range 0.2 – 2 keV, where we expect emission from the jet, we detect 120, 24 and 26 counts, respectively.

First, we fit simultaneously the spectra from EPIC pn, MOS1 and MOS2 to a number of different one-component models including a Raymond-Smith plasma (Raymond & Smith 1977), MEKAL (Mewe et al. 1985, 1986; Liedahl et al. 1995), and APEC (Smith et al. 2001), all corrected for interstellar absorption. The abundances used are those of Anders & Grevesse (1989). The fits are already very good with reduced χ^2 values between 1.185 and 1.156. The model fits show a highly absorbed hard ($kT \sim$ 11.3–13.2 keV) thermal component. The value for the column density of absorbing material is about 2.8×10^{23} cm^{-2}. The null hypothesis probability, $P_{\rm nh}$ hereafter, is between 23 and 26 %.

Since in the residuals a peak between 6 and 7 keV is visible, we fit the spectra with two components as a next step, with the same APEC model with frozen parameters and an additional Gaussian representing an emission line. The fit improve significantly, the reduced χ^2 drops to 0.722 and $P_{\rm nh}$ increases to 84 %. The center of the line is found to be at 6.08 keV with a line width of 0.23 keV. However, the fit to the norm (GS) parameter (Table 2), $2.74^{+1.63}_{-2.74} \times 10^{-6}$, shows that the data are also consistent with no line at all.

Finally we add one absorbed soft thermal component and find a temperature of $kT \sim 0.18$ and an absorbing column density of 6.1×10^{21} cm^{-2}. The reduced χ^2 drops to 0.628 and $P_{\rm nh}$ is now 92 %. The errors are somewhat larger for the parameters of this third component. We show the spectra together with this model and also the residuals in Fig. 2. The parameters of the model and their errors are also given in Table 2.

An alternative model for the hard component is based on optically thin thermal emission from an isobaric cooling flow with a maximum temperature (mkcflow in XSPEC, Mushotzky & Szymkowiak 1988). The physical picture behind this is that accreted matter is shocked inside an optically-thin boundary layer and then cools. This kind of model has been already applied successfully to a number of symbiotic stars as well as CVs (e.g. Mukai et al. 2003, and references in §4.1). Again, we first fitted the hard component only. Assuming a distance of 2.5 kpc, we set[4] the redshift to 4.16×10^{-7}. We found a temperature range in the cooling flow of 0.38 – 60.45 keV and a normalization (i.e. accretion rate in $M_\odot$ yr^{-1}) of 3.11×10^{-11}. The absorbing column density is 2.75×10^{23} cm^{-2}. The abundances are normal, 1.08 times the solar values following Anders & Grevesse (1989). The reduced χ^2 of this model is 1.82 and $P_{\rm nh}$ is 16 %. With having these parameters frozen, we added again two additional components: i) a Gaussian representing the peak between 6 and 7 keV with parameters $E = 6.10$ keV and $\sigma = 0.25$ and ii) an absorbed soft thermal component. The temperature and column density are similar to those derived before, $kT \sim 0.18$ and 6.0×10^{21} cm^{-2}. The reduced χ^2 of this model is 0.695 and $P_{\rm nh}$ is 87 %.

The total flux is almost identical throughout all of our models, covering the range (1.74–1.79)$\times 10^{-13}$ ergs cm^{-2} s^{-1}.

Although these two kinds of model are commonly used for the hard component seen in symbiotic stars, we also fitted other models to the hard component, namely i) a highly absorbed blackbody ($n_{\rm H} = 5.87 \times 10^{23}$ cm^{-2}, $kT \sim 1.11$, $\chi^2 = 0.9251$, $P_{\rm nh}$ is 57 %), ii) a highly absorbed power-law ($n_{\rm H} = 8.02 \times 10^{23}$ cm^{-2}, $\Gamma = 4.65$, $\chi^2 = 0.9235$, $P_{\rm nh}$ is 58 %). All of them give acceptable fits.

3.2. Light curves

We examined time series binned at 500 and 1000s (Fig. 3). By eye, there seems to be quasi-periodic variation on timescales of hours. The ratio of measured to expected variance is 2.781 in the 500s-binned light curve and 4.605 in the 1000s-binned time series. Hence this variability has a large statistical significance.

Within the final 4 ks of our observations, the flux increases by a factor of 2.5–4. This increase is only pronounced at energies lower than 6 keV.

We created power spectra of the full X-ray light curve of MWC 560, binned at intervals between 5 and 10 s (Fig. 4). We found several frequencies, however, the statistical significance of these peaks is not very high. The corresponding periods are in the range of stochastic flickering seen in MWC 560 in UV and optical bands (e.g. Michalitsianos et al. 1993; Tomov et al. 1996).

No hints for a periodic rapid X-ray variability are present. The fractional amplitude to which we are theoretically sensitive can be calculated using the total number of counts (624) and the number (6868) of frequencies searched (e.g. Luna & Sokoloski 2007). We find that $A \sim 0.31$, i.e. we are sensitive to oscillations with fractional amplitudes of 31 % in regions of the power spectrum dominated by white noise.

[3] See http://heasarc.gsfc.nasa.gov/docs/xanadu/xronos/xronos.html.

[4] We used a tool available at http://astronomy.swin.edu.au/~elenc/Calculators/redshift.php to calculate the corresponding redshift.

Table 2. Spectral results in the 0.1–15 keV energy range for the EPIC spectra. Errors are quoted at the 90 % confidence level for a single interesting parameter.

Model[a]	Parameter	Unit	Value	Error	
		Thermal model			
AP2G	$n_{\rm H}$	10^{22} cm^{-2}	27.87	−5.64	7.13
χ^2_r = 0.628 (d.o.f. = 26)	kT	keV	11.26	−3.44	10.59
	norm		3.01×10^{-4}	-5.98×10^{-5}	7.46×10^{-5}
	E (GS)	keV	6.08	−0.28	0.18
	σ (GS)	keV	0.23	−0.23	0.28
	norm (GS)		2.74×10^{-6}	-2.74×10^{-6}	1.63×10^{-6}
	$n_{\rm H}$	10^{22} cm^{-2}	0.61	−0.38	0.59
	kT	keV	0.18	−0.18	5.94
	norm		2.17×10^{-5}	-2.02×10^{-5}	0.47
	Total flux	ergs cm^{-2} s^{-1}	1.744×10^{-13}		
		Cooling flow model			
CF5	$n_{\rm H}$	10^{22} cm^{-2}	27.51	−2.88	3.46
χ^2_r = 0.695 (d.o.f. = 26)	$T_{\rm min}$	keV	0.38	−0.37	5.51
	$T_{\rm max}$	keV	60.45	−7.94	8.23
	Abundance		1.086	−0.85	1.21
	norm		3.11×10^{-11}	-3.46×10^{-12}	3.46×10^{-12}
	E (GS)	keV	6.10	−0.30	0.22
	σ (GS)	keV	0.25	−0.25	0.32
	norm (GS)		2.62×10^{-6}	-2.62×10^{-6}	1.71×10^{-6}
	$n_{\rm H}$	10^{22} cm^{-2}	0.60	−0.13	0.59
	kT	keV	0.18	−0.17	0.05
	norm		2.20×10^{-5}	-2.2×10^{-5}	2.3×10^{-5}
	Total flux	ergs cm^{-2} s^{-1}	1.792×10^{-13}		

[a] Models applied in XSPEC notation:
AP2G = wabs(apec)+wabs(apec+gaussian) (Abundance = 1, redshift = 0)
CF5 = wabs(apec)+wabs(gaussian+mkcflow) (Redshift = 4.16×10^{-7}, switch = 0)

4. Discussion

4.1. The hard component of the spectrum

The first model fits show a highly absorbed hard ($kT \sim$ 11.3–13.2 keV) thermal component. The value for the column density of absorbing material, 2.8×10^{23} cm^{-2}, is very high. Models of visual interstellar absorption towards MWC 560 give much lower values: $n_H = 1.5\times10^{21}$ cm^{-2} (Hakkila et al. 1997), $n_H = 3.07\times10^{21}$ cm^{-2} (Kalberla et al. 2005) or $n_H = 3.25\times10^{21}$ cm^{-2} (Dickey & Lockman 1990). Thus the absorption must be caused by material close to the central white dwarf. Our own calculations showed that the column density of the jet is only of the order of 10^{22} cm^{-2} (Stute & Camenzind 2005; Schmid et al. 2001) or below, thus the high column density derived from our data cannot be attributed to the jet.

MWC 560 seems to well fit in the class of symbiotic stars with a hard X-ray component. Both the amount of absorbing material and the temperature of the hard component we found in MWC 560 using a thermal model are close to values seen in similar objects as CH Cyg ($n_H = 3.2\times10^{23}$ cm^{-2}, 10 keV; Mukai et al. 2007), SS7317 ($n_H = 1.6\times10^{23}$ cm^{-2}, 9.3 keV; Smith et al. 2008) and R Aqr ($n_H = 3.5\times10^{23}$ cm^{-2}, 6.8 keV; Nichols et al. 2007). We also fit the spectra with a cooling flow model and find a maximum temperature of 61 keV in MWC 560 which is similar to those in RT Cru (80 keV; Luna & Sokoloski 2007) and T CrB (57 keV; Luna et al. 2007). This may be a hint that the masses of the white dwarf in these objects are comparable, since the maximum temperature is determined by the depth of the potential well around the white dwarf and thus by its compactness.

We infer from our X-ray data that in MWC 560 the accretion rate is $3.1\times10^{-11}\,(d/2.5{\rm kpc})^2$ M$_\odot$ yr^{-1}, significantly lower than in T CrB (4.2×10^{-9} M$_\odot$ yr^{-1}, Luna et al. 2007) and RT Cru (1.8×10^{-9} M$_\odot$ yr^{-1}, Luna & Sokoloski 2007), two objects without jets, and also much lower than in CH Cyg, which does have jets. With a mean flux of the hard energy component of about 1.6×10^{-13} ergs cm^{-2} s^{-1}, MWC 560 has an about 10 times lower flux than the hard X-ray component of CH Cyg during the faint state in 2006 and even an about 420 times lower flux during CH Cyg's bright state in 1994 (Mukai et al. 2007). Since CH Cyg is about ten times closer than MWC 560, a factor of 100 would be expected, if both objects had the same accretion rate.

We hypothesise that MWC 560's accretion rate is variable and that MWC 560 switches between faint and bright states as seen in e.g. neutron star X-ray binaries and also CH Cyg. This hypothesis is supported by Schmid et al. (2001)'s determination of an accretion rate of 5×10^{-7} M$_\odot$ yr^{-1} from ultraviolet data. This high rate is consistent with a jet outflow rate of about 7×10^{-9} M$_\odot$ yr^{-1} at the time of their spectroscopic observations, assuming that a few percent of the accreted material is being ejected in the jet.

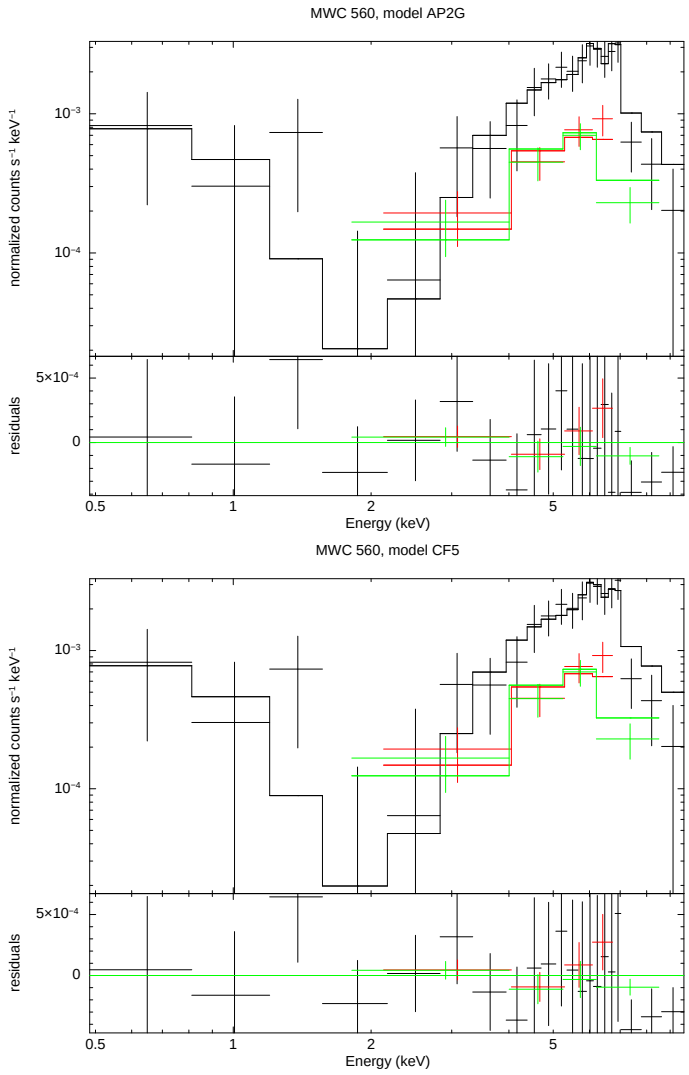

Fig. 2. Observed spectrum of MWC 560 together with several models: our best fit models with an absorbed soft APEC model and another absorbed hard APEC model plus a Gaussian (top) and an optically thin thermal emission from an isobaric cooling flow with a maximum temperature plus a Gaussian, both absorbed, and an additional absorbed soft thermal component (bottom); also shown are the residuals for each fit. The colors correspond to different instruments: PN (black), MOS1 (red), MOS2 (green)

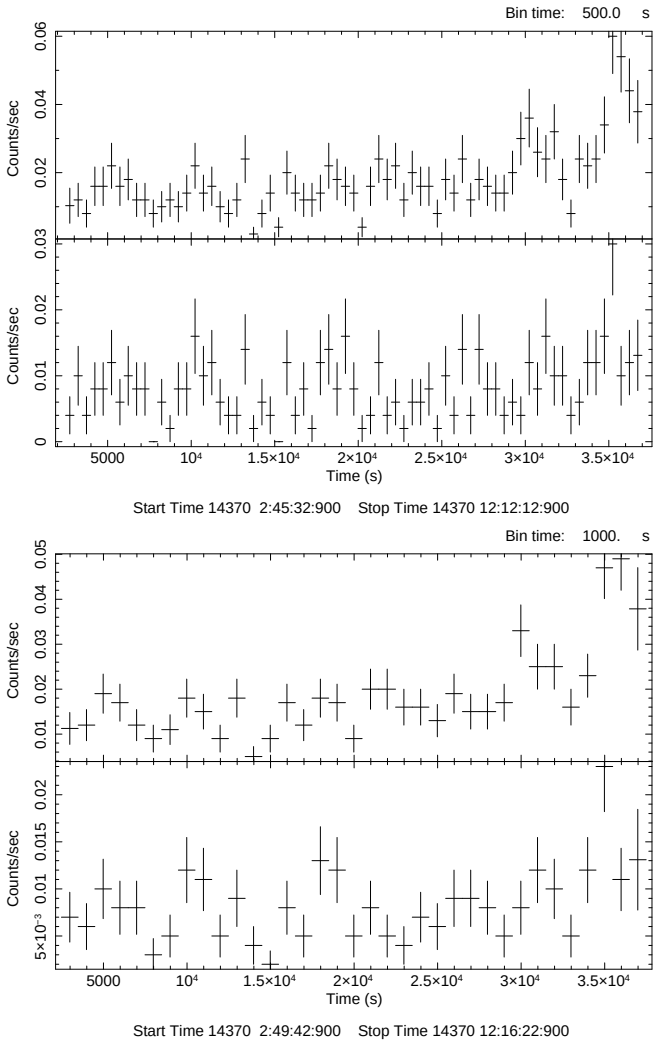

Fig. 3. PN light curves binned at 500s and 1000s for energies between 0.3–15 keV (top) and between 6–15 keV (bottom).

In our fits, we added a Gaussian representing an emission line. We found a central energy of ∼ 6.1 keV and a width of ∼ 0.25 keV. Usually, the following lines are detected: a Fe Kα fluorescence line at 6.4 keV or Fe XXV and XXVI emission lines at 6.7 and 6.97 keV, respectively. Only the first of these lines is consistent with our fits, since the error of the peak energy is large, 0.3 keV. However, the large errors of the line strength (see "norm (GS)", Table 2, both models) found in our fits suggest that the data are also consistent with no line being present.

4.2. The soft jet component(s)

In Stute & Sahai (2007), we modeled the X-ray emission which we can expect from the jet in MWC 560, according to our models of Stute (2006). We found that the synthetic jet spectrum can be described with a hot and a warm optically-thin plasma component. During the minima (maxima) of the X-ray emission light cycle, the hot component is predicted to have a temperature of ∼0.7 keV (1.6 keV); the warm component has temperature values of ∼0.14 keV (0.33 keV). The total X-ray luminosity found in our best-fit simulation using the optical data (model iv'; Stute 2006) decreased with time from an initial value of about $5{\times}10^{-12}$ ergs cm^{-2} s^{-1} directly after the emergence of the jet. Note that we modeled only 115 days in model iv' due to computational constraints. The X-ray luminosity is proportional to the density of the shocked material and to the shock velocity. At the beginning, the density contrast as well as the velocity difference between the jet and the slow ambient medium are the highest. After some time, however, the fast wind does not plow into the ambient medium anymore, but into previously ejected fast wind material with more similar density and velocity values as the unshocked fast wind itself. At the same time the jet expands also in its lateral direction away from the symmetry axis, i.e. lateral kinetic energy becomes an important sink of energy and the conversion factor of input kinetic energy into X-ray luminosity decreases. Both factors cause the decline in the X-ray luminosity seen in the simulations. Superimposed on the global decline, a cycle with a period of 7-day and amplitudes of about 20 % was present.

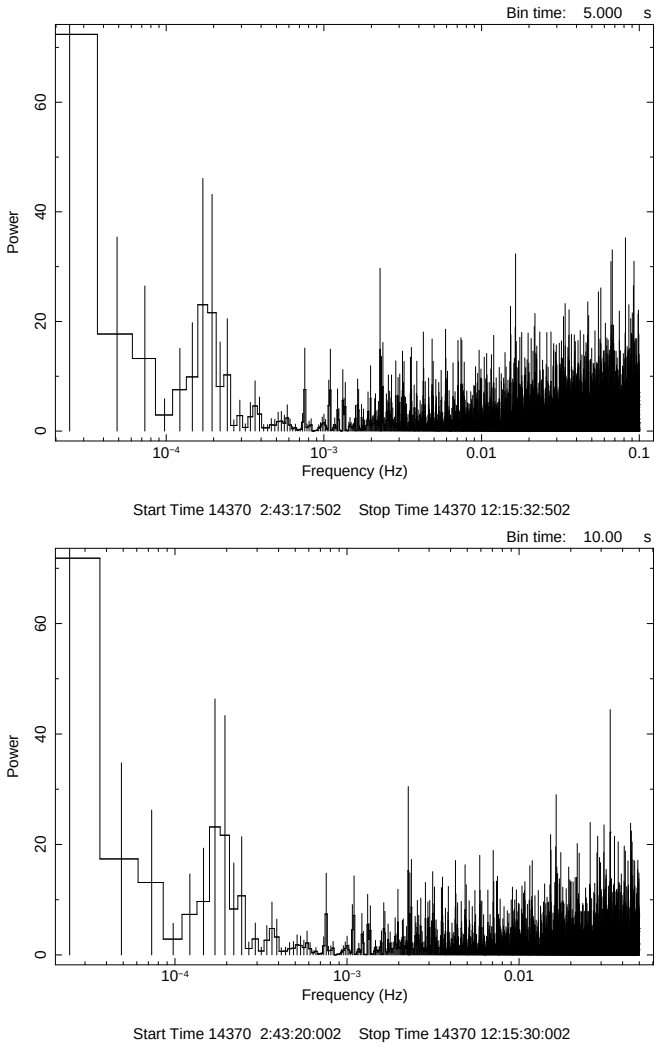

Fig. 4. Power spectra of the pn X-ray light curve of MWC 560, binned at 5 and 10 *s*, respectively.

Between 0.2 keV and 3 keV, the observed flux is about 10^{-15} ergs cm^{-2} s^{-1}. Hence Mürset et al. (1997)'s sensitivity was with their lower limit of 8×10^{-15} ergs cm^{-2} s^{-1} just below of what had been needed to detect MWC 560. Therefore the highest possible decline, if any, of the soft X-ray emission is about a factor of eight within the 15 years from the ROSAT observations in April 1992 and our observations in September 2007. The observations of Merrill & Burwell (1943), where blue-shifted absorption features near the emission lines of HI and Ca II K were already noticed, set a lower limit on the age of the jet of about 60 yrs.

The ROSAT All-Sky Survey Faint Sources catalog lists a source, 1RXS J072546.4-074342, 1RXS hereafter, which lies 77" away from the SIMBAD position of MWC 560. Its count rate in October 1990 was 0.0149 counts s^{-1} (a flux of 1.7×10^{-13} ergs cm^{-2} s^{-1}), i.e. the flux is 100 times higher than our observed flux. In Fig. 5, we plot our full XMM pn field of view (left) and the same field of view within the ROSAT observation of Mürset et al. (1997) in April 1992 (right). We also identified the three closest sources listed in the ROSAT All-Sky Survey Faint Sources catalog. For all these source, we can find counterparts at the correct position in the ROSAT and XMM observations. The source 1RXS is not present in either of them. Thus, 1RXS has a large and variable X-ray flux, highlighting its potential importance as an X-ray transient source. However, due to the absence of obvious pointing errors between XMM and ROSAT data, we conclude that 1RXS is not the same source as MWC560.

The observed temperature of the soft component, $kT \sim 0.18$, is slightly lower than predicted by our simulations. The observed flux values between 0.2 keV and 3 keV are more than a factor 100 less than predicted by our models (1.6×10^{-13} erg s^{-1} cm^{-2} between 0.1 – 2.4 keV), and clearly cannot be due to coincidentally catching the MWC560 jet at the minimum of the 7-day flash cycle. Extrapolating the global decline in our models, however, shows that the flux from the jet can drop to the observed fluxes within several years after the emergence of the jet, if we assume that the jet emission follows the same ejection pattern as in our models.

Although we know that a jet is present in MWC 560 and requiring only the jet for explaining the observed soft component is tempting, there are other scenarios for producing soft or even supersoft X-rays. A component with a temperature of about 0.2 keV is also typical for photospheric emission from very hot white dwarfs (e.g. Jordan et al. 1994). Soft components which peak around 0.8–1 keV are produced by several kinds of shocks with shock velocities of about 1000 km s^{-1}, present not only in jets, but also in colliding winds and during the accretion process.

We note that our soft component is resolved in only three energy bins, since we required at least 25 counts per bin. This makes it difficult to fit this component in a reliable manner and so the resulting constraints on our jet model are very weak or non-existent. Furthermore it is not possible to distinguish between the above mentioned scenarios producing supersoft or soft X-ray emission. We have to obtain more data by observing MWC 560 again with either Chandra or XMM.

4.3. The timing analysis

We detected quasi-periodic flickering on timescales of minutes and hours, which usually emanates from an accretion region close to the white dwarf. Accretion thus seems to power the detected X-ray emission. One open question, however, is whether the white dwarf is magnetized or not. In the first case, the hard component is emitted by accretion columns. The disk will be truncated, the BL disappears and matter falls freely along magnetic field lines towards the magnetic poles. The infalling matter then forms a strong shock near the white dwarf surface leading to optically-thin hard X-ray emission with $kT \sim 10 - 20$ keV (e.g. Cropper et al. 2000). Also the presence of rapid *periodic* variability with the Keplerian period at the truncation radius would be very likely. If the white dwarf is not magnetized , the hard component is emitted by an optically-thin boundary layer (Pringle & Savonije 1979; Popham & Narayan 1995). Since we did not detect periodic variability, we favor this possibility.

The increase seen at the end of our previous observation may (i) be related to the emergence of a new high-velocity pulse creating an X-ray flash as seen in our simulations, (ii) represent a secular increase, or (iii) be due to switching to a "bright" state from a "faint" one, as seen in CH Cyg – only new observations can distinguish between these alternatives.

5. Conclusion

We discovered X-ray emission from MWC 560 using XMM-Newton. We found spectra consisting of two distinct components, a soft and a hard component. Thus MWC 560 is the newest member of a new sub-class of symbiotic stars emitting hard X-rays with similar parameters.

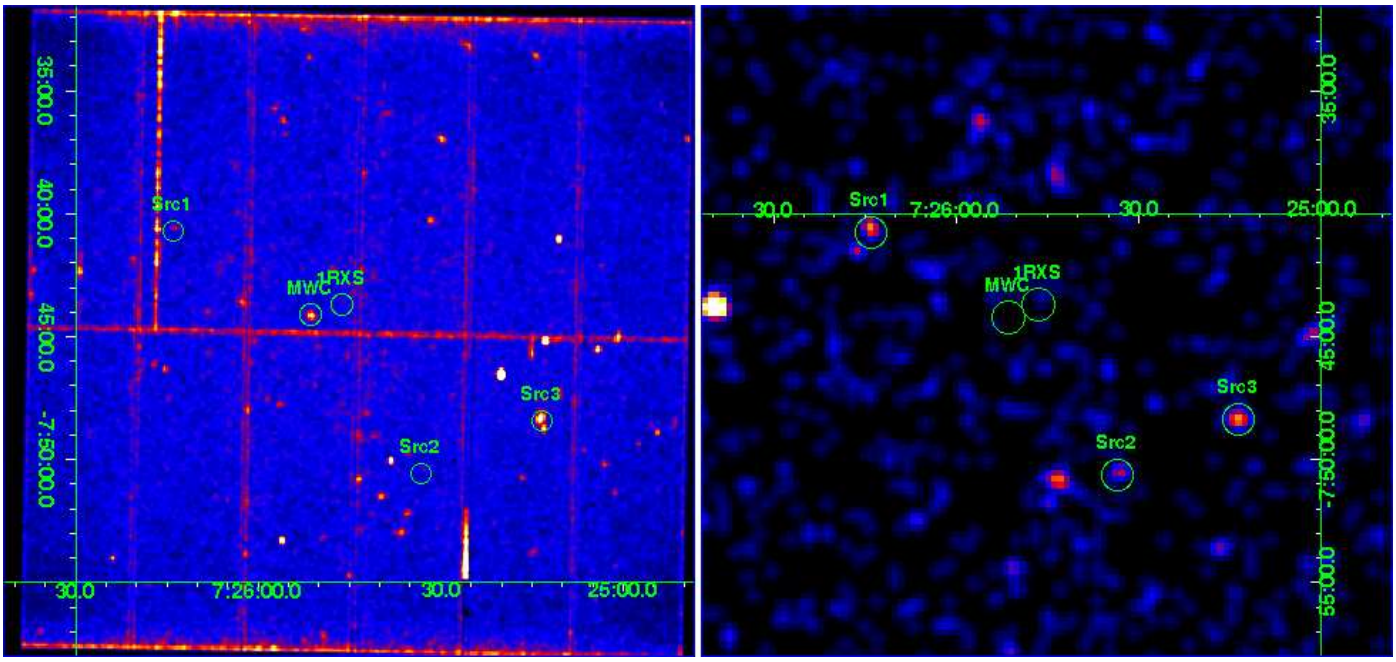

Fig. 5. Images from our full XMM pn field of view (left) and the same field of view within the ROSAT observation of Mürset et al. (1997) (right). Also plotted are the three closest sources listed in the ROSAT All-Sky Survey Faint Sources catalog (Src1: 1WGA J0726.2-0740, Src2: 1WGA J0725.5-0750, Src3: 1WGA J0725.2-0748). For all these source, we can find counterparts at the correct position in the ROSAT and XMM observations. The source 1RXS is not present in either of them. MWC 560 has not been detected by ROSAT.

From modelling the hard component, the absence of periodic variability and the presence of short-term flickering, we conclude that the hard component is emitted by an optically-thin boundary layer around a high-mass white dwarf.

We hypothesise that MWC 560's accretion rate is variable and that MWC 560 switches between faint and bright states as seen in e.g. neutron star X-ray binaries and also CH Cyg.

Due to low photon counts in the soft component, it is difficult to fit this component in a reliable manner. Furthermore it is not possible to distinguish between several scenarios producing supersoft or soft X-ray emission. On the other hand, the soft X-ray flux, significantly smaller than predicted by our models at the emergence of the jet, still provided a strong constraint on our simulations, testing of which was the main goal of the presented observations.

More observational data with either XMM or Chandra are needed as well as further simulations with longer time baselines.

Acknowledgements. We acknowledge helpful and improving comments and suggestions by the referee. The present work was supported in part by the European Community's Marie Curie Actions - Human Resource and Mobility within the JETSET (Jet Simulations, Experiments and Theory) network under contract MRTN-CT-2004 005592 (MS). RS thanks NASA for funding this work by XMM-Newton AO-6 award NMO710766-103905, an LTSA award (NMO710840-102898); RS also received partial support for this work from an HST GO award (no. GO-10317.01) from the Space Telescope Science Institute (operated by the Association of Universities for Research in Astronomy, Inc., under NASA contract NAS5-26555). Some of the research described in this paper was carried out by RS at the Jet Propulsion Laboratory, California Institute of Technology, under a contract with the National Aeronautics and Space Administration.

References

Anders, E., Grevesse, N. 1989, GeCoA, 53, 197
Belczynski K., Mikolajewska J., Munari U., et al. 2000, A & AS, 146, 407
Blandford, R. D., Payne, D. G. 1982, MNRAS, 199, 883
Brocksopp, C., Sokoloski, J. L., Kaiser, C., et al. 2004, MNRAS, 347, 430
Cropper, M., Wu, K., Ramsay, G. 2000, New AR, 44, 57
Dickey, J. M., Lockman, F. J. 1990, ARA & A, 28, 215
Ezuka, H., Ishida, M., Makino, F. 1998, ApJ, 499, 388
Eyres, S. P. S., Bode, M. F., Skopal, A., et al. 2002, MNRAS, 335, 526l
Galloway, D. K., Sokoloski, J. L. 2004, ApJ, 613, L61
Hakkila, J., Myers, J. M., Stidham, B. J., Hartmann, D. H. 1997, AJ, 114, 2043
Hollis, J.M., Michalitsianos, A. G., Kafatos, M., et al. 1985, ApJ, 289, 765
Hollis, J. M., Lyon, R. G., Dorband, J. E., et al. 1985, ApJ, 475, 231
Hünsch, M., Schmitt, J. H., Schroeder, K., Zickgraf, F. 1998, A & A, 330, 225
Jordan S., Mürset U., Werner K. 1994, A & A, 283, 475
Kalberla, P. M. W., Burton, W. B., Hartmann, D., et al. 2005, A & A, 440, 775
Karovska, M., Carilli, C. L., Raymond, J. C., Mattei, J. A. 2007, ApJ, 661, 1048
Kellogg, E., Pedelty, J. A., Lyon, R. G. 2001, ApJ, 563, 151
Kellogg, E., Anderson, C., Korreck, K, et al. 2007, ApJ, 664, 1079
Leahy, D. A., Taylor, A. R. 1987, A & A, 176, 262
Liedahl D. A., Osterheld A. L., Goldstein W. H. 1995, ApJ, 438, L115
Luna, G. J. M., Sokoloski, J. L. 2007, ApJ, 671, 741
Luna, G. J. M., Sokoloski, J. L., Mukai, K. 2007, arXiv0711.0725
Mason, K. O., Breeveld, A., Much, R., et al. 2001, ApJ, 365, L36
Merrill, P. W., Burwell, C. G. 1943, ApJ, 98, 153
Mewe R., Gronenschild E. H. B. M., van den Oord G. H. J. 1985, A & AS, 62, 197
Mewe R., Lemen J. R., van den Oord G. H. J. 1986, A & AS, 65, 511
Michalitsianos, A. G., Perez, M., Shore, S. N., Maran, S. P., Karovska, M., Sonneborn, G., Webb, J. R., Barnes, Thomas G., III, Frueh, M. L., Oliversen, R. J.. Starrfield, S. G. 1993, ApJ, 409, 53
Mushotzky R. F., Szymkowiak A. E. 1988, in: Cooling Flows in Clusters and Galaxies ed. A. C. Fabian, p. 53
Mukai, K., Kinkhabwala, A., Peterson, J. R., et al. 2003, ApJ, 586, L77
Mukai, K., Ishida, M., Kilbourne, C., et al. 2006, PASJ, 59, 177
Mürset, U., Wolff, B., Jordan, S. 1997 , A & A, 319, 201
Nichols, J. S., DePasquale, J., Kellogg, E., et al. 2007, ApJ, 660, 651
Paresce, F., Hack, W. 1994, A & A, 287, 154
Popham, R., Narayan, R. 1995, ApJ, 442, 337
Pringle, J. E., Savonije, G. J. 1979, MNRAS, 187, 777
Raymond J. C., Smith B. W. 1977, ApJS, 35, 419
Schmid, H. M., Kaufer, A., Camenzind, M., et al. 2001, A & A, 377, 206
Smith R. K., Brickhouse N. S., Liedahl D. A., Raymond J. C., 2001, ApJ, 556, L91
Smith, R. K., Mushotzky, R., Mukai, K., Kallman, T., Markwardt, C. B., Tueller, J. 2008, PASJ, 60, 43

Soker, N., Lasota, J.-P. 2004, A & A, 422, 1039
Solf, J., Ulrich, H. 1985, A & A, 148, 274
Strüder L., Briel U., Dennerl K. et al., 2001, A & A, 365, L18
Stute, M., 2006, A & A, 450, 645
Stute, M., Camenzind, M. 2005, A & A, 432, L17
Stute, M., Sahai, R. 2007, ApJ, 665, 698
Stute, M., Camenzind, M., Schmid, H. M. 2005, A & A, 429, 209
Taylor, A. R., Seaquist, E. R., Mattei, J. A. 1986, Nature, 319, 38
Tomov, T., Kolev, D., Zamanov, R., Georgiev, L., Antov, A. 1990, Nature, 346, 637
Tomov, T., Kolev, D., Ivanov, M., Antov, A., Jones, A., Mikolajewski, M., Lepardo, A., Passuello, R., Saccavino, S., Sostero, G., Valentinuzzi, T., Bellas-Velidis, Y., Dapergolas, A., Munari, U. 1996, A & AS, 116, 1
Turner M. J. L., Abbey A., Arnaud M. et al., 2001, A & A, 365, L27
Viotti, R., Piro, L., Friedjung, M., Cassatella, A. 1987, ApJ, 319, L7
Wheatley, P. J., Kallman, T. R. 2006, MNRAS, 372, 1602